PHOTONICS Research

Kelly sideband suppression and wavelength tuning of a conventional soliton in a Tm-doped hybrid mode-locked fiber laser with an all-fiber Lyot filter

Jianfeng Li,[1,*] Yazhou Wang,[1] Hongyu Luo,[1] Yong Liu,[1] Zhijun Yan,[2,4] Zhongyuan Sun,[3] and Lin Zhang[3,5]

[1]State Key Laboratory of Electronic Thin Films and Integrated Devices, School of Optoelectronic Science and Engineering, University of Electronic Science and Technology of China, Chengdu 610054, China
[2]School of Optical and Electronic Information, Huazhong University of Science and Technology, Wuhan 430074, China
[3]Aston Institute of Photonic Technologies (AiPT), Aston University, Birmingham B4 7ET, UK
[4]e-mail: yanzhijin@gmail.com
[5]e-mail: l.zhang@aston.ac.uk
*Corresponding author: lijianfeng@uestc.edu.cn

Received 23 August 2018; revised 1 November 2018; accepted 19 November 2018; posted 20 November 2018 (Doc. ID 343083); published 7 January 2019

We demonstrate a stable conventional soliton in a Tm-doped hybrid mode-locked fiber laser by employing a homemade all-fiber Lyot filter (AFLF) and a single-wall carbon nanotube. The AFLF, designed by sandwiching a piece of polarization-maintained fiber (PMF) with two 45° tilted fiber gratings inscribed by a UV laser in PMF with a phase-mask scanning technique, shows large filter depth of ~9 dB and small insertion loss of ~0.8 dB. By optimizing the free spectral range of the AFLF, the Kelly sidebands of a conventional soliton centered at 1966.4 nm can be dramatically suppressed without impairing the main shape of the soliton spectrum. It gives the pulse duration of 1.18 ps and bandwidth of 3.8 nm. By adjusting the temperature of the PMF of the AFLF from 7°C to 60°C, wavelength tunable soliton pulses ranging from 1971.62 nm to 1952.63 nm are also obtained. The generated soliton pulses can be precisely tuned between 1971.62 nm and 1952.63 nm by controlling the temperature of the AFLF.

https://doi.org/10.1364/PRJ.7.000103

1. INTRODUCTION

The 2 μm optical soliton generated from mode-locked fiber lasers has attracted wide attention because of its wide applications, such as mid-IR supercontinuum generation and remote sensing. Various nanomaterials such as a semiconductor saturable absorption mirror, a single-wall carbon nanotube (SWCNT), graphene, a topological insulator, and black phosphorus can be used as a "slow" saturable absorber (SA) to initiate and stabilize mode-locked fiber lasers [1–5]. However, their slow response leads to a long pulse tail for the mode-locked pulse and thus enlarges the pulse duration [6–8]. In comparison, artificial fast SAs formed by nonlinear polarization evolution (NPE), a nonlinear amplifying loop mirror, or a nonlinear optical loop mirror have the advantages of a large modulation depth and the instantaneous response of a Kerr medium (~10 fs for silica glass) [9], and permit a broad running bandwidth and thus narrower pulse duration. Nonetheless, lasers mode locked by the fast SA have difficulty in self-starting a single pulse due to the demand of the high nonlinearity effect [10,11], and they are sensitive to environmental vibrations. Alternatively, a hybrid mode-locked mechanism that incorporates both "slow" and "fast" SAs permits generating self-starting ultrashort pulses with narrower pulse duration [11]. Exploiting this mechanism, the slow SA facilitates pulse initiation and stabilizes the laser operation, while the fast SA acts as the pulse shaper to ensure pulse quality in the steady state regardless of the slow SA characteristics [1,12].

On the other hand, because of the lack of a normal dispersion fiber component, a conventional soliton operating in the anomalous dispersion regime is the universal soliton regime at this wavelength band [13]. The formation of this soliton regime is accompanied by sharp spectral Kelly sidebands, which are caused by resonant enhancement between the dispersive and soliton waves [14]. The Kelly sidebands are distributed symmetrically around the pulse's spectral center peak, and their space is decided by the total dispersion value of the fiber

cavity [10,15]. Kelly sidebands can cause interaction of adjacent soliton pulses because of their large temporal width compared with the pulse width [16]. Such an interaction leads to pulse timing jitter, which not only reduces the stability of the mode-locked fiber laser but also generates excess bit errors over long-distance propagation [17]. The strong Kelly sidebands with energy comparable to the pulse itself also imply a possible limitation on soliton amplification efficiency [18]. Due to these disadvantages of the Kelly sidebands, several methods have been proposed to suppress Kelly sidebands. By shortening the cavity length, the wavelengths of Kelly sidebands have been moved out of the erbium gain region [19]. Two polarizers separated by approximately a half roundtrip have been used to filter the dispersive wave [20]. The Kelly sidebands can also be prevented by designing the laser cavity so that its length is longer than the soliton period of the pulses [21]. A simpler and common method is the use of a band-pass filter with an appropriate bandwidth. Although some typical filters such as the Fabry–Perot filter and birefringent plate filter have been used to suppress the Kelly sidebands in the 1.5 μm band [22,23], their complicated space structure and large insertion loss limit practical applications. In order to effectively suppress the Kelly sidebands in a mode-locked oscillator, a filter designed with adjustable bandwidth and large filter depth is desirable. Especially for a mode-locked fiber laser, the flexible cavity dispersion allows a large range of wavelength separation between a Kelly sideband and soliton spectral peak, indicating that the free spectral range (FSR) of the filter should be easily adjusted according to the practical case. There is a series of types of all-fiber filters, such as a fiber birefringence induced comb filter [24–26], fiber taper [26,27], chirped fiber Bragg grating [28], and all-fiber Lyot filter (AFLF) [29,30]. Among them, the AFLF, composed of a piece of polarization-maintained fiber (PMF) sandwiched between two PMF-based 45° tilted fiber gratings (45°-TFGs), is a suitable candidate possessing the advantages of controllable FSR and large filtering depth. In addition, the AFLF exhibits thermal tuning ability for the operation wavelength and high polarization extinction ratio [29,31]. The former advantage allows precise wavelength tunability by controlling the temperature of the AFLF, while the latter advantage facilitates the NPE mode locking without an additional polarizer. Inspired by these advantages, the AFLF has been intensively studied and used at 1–1.5 μm [31,32], improving the flexibility and performance of mode-locked fiber lasers. However, due to the difficulty of the PMF-based 45°-TFG fabrication technique in the 2 μm band, an AFLF has never been reported in this spectral region.

Here, a conventional soliton with suppressed Kelly sidebands is demonstrated in a Tm-doped mode-locked fiber laser by using a homemade AFLF. Hybrid mode locking combining NPE and SWCNT is employed to improve the performance of the conventional soliton. The AFLF shows a large filtering depth of ~9 dB and small insertion loss of ~0.8 dB. The FSR of the AFLF is optimized to effectively filter out the Kelly sidebands without impairing the main shape of the soliton spectrum. The soliton can also be precisely tuned by controlling the temperature of the AFLF.

2. PREPARATION OF THE AFLF

A. Numerical Model

Figure 1(a) shows the configuration of our homemade AFLF. It consists of a section of PMF cavity at an angle of 45° between the same two 45°-TFGs inscribed in PMF with respect to their

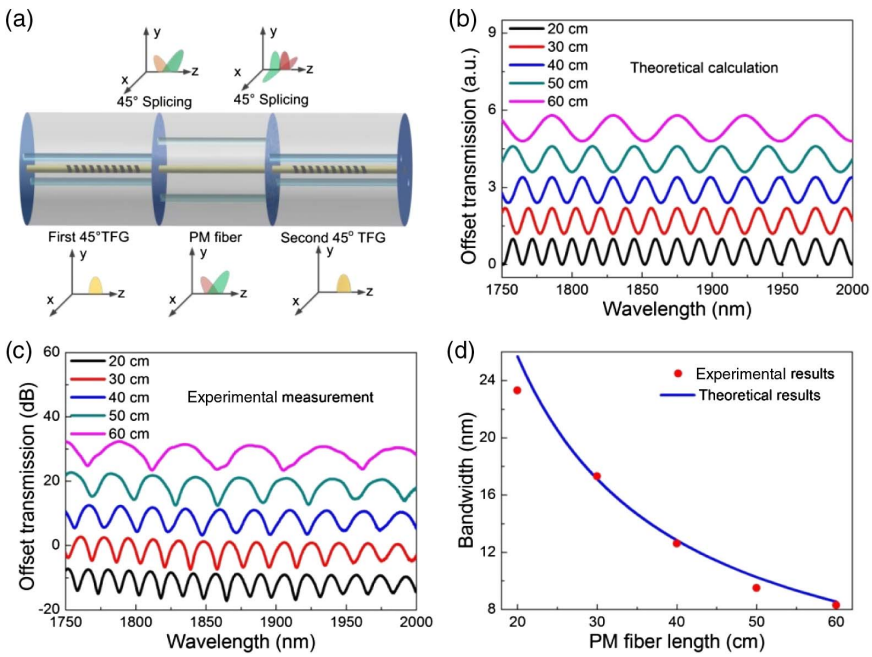

Fig. 1. (a) Configuration of our AFLF consisting of two 45°-TFGs segmented by a PMF cavity and corresponding polarization state and phase delay evolutions as the light passes through each portion (inset); (b) theoretically calculated and (c) experimentally measured transmission spectra using PMFs with different lengths of 20 cm, 30 cm, 40 cm, 50 cm, and 60 cm; and (d) experimentally measured and theoretically calculated bandwidths of the AFLF as a function of the PMF length.

fast or slow axes. Note that the fast or slow axes of the two 45°-TFGs are in parallel in the structure. Specifically, the linearly polarized beam along the fast or slow axis of the first 45°-TFG will be divided into two vertical linearly polarized beams with equal amplitudes at the start of the PMF. Then the two beams experience different phase delays when propagating in the PMF and then will be combined again when going into the second 45°-TFG, resulting in interference with maximum visibility. According to the structure of the AFLF, the transfer matrix can be expressed by Jones matrices:

$$M = \begin{bmatrix} \sin^2\beta & \cos\beta\sin\beta \\ \sin\beta\cos\beta & \cos^2\beta \end{bmatrix} \times \begin{bmatrix} e^{-i\Delta\varphi}\cos^2\alpha + \sin^2\alpha & (e^{-i\Delta\varphi}-1)\cos\alpha\sin\alpha \\ (e^{-i\Delta\varphi}-1)\cos\alpha\sin\alpha & e^{-i\Delta\varphi}\sin^2\alpha + \cos^2\alpha \end{bmatrix} \times \begin{bmatrix} 0 & 0 \\ 0 & 1 \end{bmatrix} \begin{bmatrix} 1 \\ 1 \end{bmatrix}, \quad (1)$$

where matrix $\left[\begin{smallmatrix}1\\1\end{smallmatrix}\right]$ is for incident light, matrix $\left[\begin{smallmatrix}0&0\\0&1\end{smallmatrix}\right]$ is for the first 45°-TFG, matrix $\left[\begin{smallmatrix}e^{-i\Delta\varphi}\cos^2\alpha+\sin^2\alpha & (e^{-i\Delta\varphi}-1)\cos\alpha\sin\alpha \\ (e^{-i\Delta\varphi}-1)\cos\alpha\sin\alpha & e^{-i\Delta\varphi}\sin^2\alpha+\cos^2\alpha\end{smallmatrix}\right]$ is for the PMF, and matrix $\left[\begin{smallmatrix}\sin^2\beta & \cos\beta\sin\beta \\ \sin\beta\cos\beta & \cos^2\beta\end{smallmatrix}\right]$ is for the second 45°-TFG. The fast axis of the first 45°-TFG is set as the x axis; therefore, α and β are the angles between the x axis and the fast axes of the PMF and the second 45°-TFG, respectively. $\Delta\varphi$ is the phase difference induced by the PMF. According to Eq. (1), the normalized transmission spectrum of the AFLF is

$$T = \cos^2(2\alpha+\beta) + \cos^2(\Delta\varphi/2)\sin 2\alpha \sin 2(\alpha+\beta), \quad (2)$$

$$\Delta\varphi = \frac{2\pi L_{\mathrm{PM}}\Delta n}{\lambda}, \quad (3)$$

where L_{PM} and Δn are the length and birefringence of the PMF, respectively. It is observed that the maximum or minimum transmission is obtained when $\Delta\varphi = 2m\pi$ or $(2m+1)\pi$ ($m = 0, 1, 2, 3$). Therefore, the maximum and minimum transmission can be expressed as

$$T_{\max} = \mathrm{Max}[\cos^2\beta, \cos^2(2\alpha+\beta)],$$
$$T_{\min} = \mathrm{Max}[\cos^2\beta, \cos^2(2\alpha+\beta)]. \quad (4)$$

In order to obtain maximum modulation depth, β should be equal to 0° or 90°, while α is equal to 45°. In this case, we take $\beta = 0°$ and $\alpha = 45°$ as an example; the relative transmission spectrum can be simplified as follows:

$$T = \cos^2(\Delta\varphi/2). \quad (5)$$

Based on Eq. (5), the wavelength corresponding to maximum and minimum transmission can be expressed as

$$\lambda^m_{\max} = \frac{L_{\mathrm{PM}}\Delta n}{m}, \quad \lambda^m_{\min} = \frac{2L_{\mathrm{PM}}\Delta n}{2m+1}, \quad (6)$$

and the FSR of the AFLF is calculated to be

$$\mathrm{FSR} \cong \frac{\lambda^2}{L_{\mathrm{PM}}\Delta n}. \quad (7)$$

It is well known that the birefringence of PMF is induced by the tension generated from the high thermal expansion of the two rods placed around the fiber core. By subjecting the PMF to a raised temperature, the interior tension would be released, thus leading to decreased birefringence.

Because the interior tension of the PMF will be released by increasing the temperature of the fiber, the spectrum response of the AFLF can be precisely tuned by controlling its temperature [30]. By differentiating Eq. (6), the wavelength shift of the mth minimum transmission band of the AFLF induced by the temperature is expressed as

$$\mathrm{d}\lambda^m_{\min} = \frac{L_{\mathrm{heating}}\lambda^m_{\min}}{L_{\mathrm{PM}}}\left(\frac{\mathrm{d}L_{\mathrm{heating}}}{L_{\mathrm{heating}}\mathrm{d}T} + \frac{\mathrm{d}\Delta n}{\Delta n \mathrm{d}T}\right)\Delta T, \quad (8)$$

where L_{heating} is the effective length of the PM fiber under heating, $\frac{\mathrm{d}L_{\mathrm{heating}}}{L_{\mathrm{heating}}\mathrm{d}T}$ is the thermal expansion coefficient, which is 0.5×10^{-6} for silica fiber, and $\frac{\mathrm{d}\Delta n}{\Delta n \mathrm{d}T}$ is the thermal optical coefficient of birefringence of the PM fiber. In our case, it is evaluated to be -1.3×10^{-3} by measuring the temperature sensitivity of a fiber Bragg grating (FBG) made in the same PM fiber.

B. Fabrication

In the fabrication, first, the 45°-TFG centered at ~1950 nm is UV inscribed into a section of commercial PMF (Thorlabs, PMF 2000) with a beat length of 5.2 mm using the standard phase-mask scanning technique. The inscription UV laser is a 244 nm UV source from a continuous-wave frequency doubled Ar^+ laser (Coherent Sabre Fred). The phase mask (Ibsen, Denmark) has a 25 mm long uniform pitch and 33.7° tilted angle with respect to the fiber axis. It can produce the internal titled index fringes at 45° in the fiber core with a polarizing function response to a broadband light around 1950 nm. Before the inscription, the PMF is hydrogen loaded at 150 bar (1 bar = 100 kPa) at 80°C for 48 h to enhance its photosensitivity. After the inscription, the grating samples are subjected to an annealing treatment at 80°C for 48 h to stabilize the grating structure. Then splicing a section of the same PMF at an angle of 45° between two 45°-TFGs with respect to their fast or slow axes forms an AFLF with the maximum modulation depth.

C. Testing of AFLF Performance

According to Eq. (7), the FSR of the AFLF can be adjusted flexibly by varying the PMF length. Figures 1(b) and 1(c) show the theoretically calculated and experimentally measured transmission spectra of five AFLFs using PMF lengths of 20 cm, 30 cm, 40 cm, 50 cm, and 60 cm operated at room temperature. The experimental transmission spectra are obtained by injecting a homemade Tm-doped fiber amplified spontaneous emission (ASE) source into the AFLF. It is observed that the measured transmission spectra exhibit comb-like profiles with modulation depths of ~9 dB. Figure 1(d) shows the FSR of the AFLF as a function of the PMF length; it decreases nonlinearly from 23.3 nm to 8.3 nm for the PMF length from 20 cm to 60 cm, which is consistent with the theoretical result. The insertion loss of the AFLF is measured to be ~0.8 dB, comparable to commercial filters, which is caused mainly by the mode mismatch between the PMF and SMF28e fiber. If the AFLF is used in a PMF laser, the insertion loss will be reduced significantly. Moreover, the AFLF also acts as a polarizer. As a polarizer, its insertion loss is smaller than commercial polarizers with a typical insertion loss of ~1.0 dB. Therefore, for mode-locked

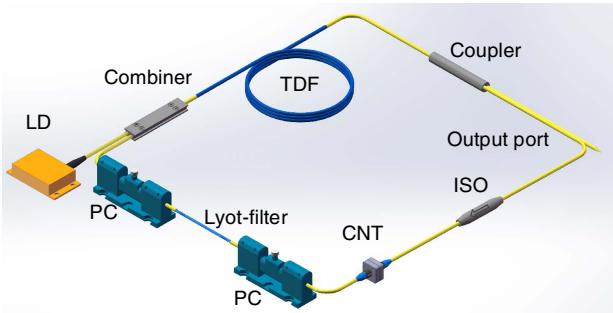

Fig. 2. Experimental setup of hybrid mode-locked Tm-doped fiber laser based on an AFLF.

fiber lasers, the AFLF playing as both the filter and the polarizer is actually favorable to reduce the total insertion loss.

3. EXPERIMENTAL SETUP OF MODE-LOCKED OSCILLATOR

Figure 2 shows the setup of the AFLF-based hybrid mode-locked fiber laser. A 2.0 m double-clad Tm-doped fiber (Coractive, DCF-TM-10/128) with an octagonal-shaped inner cladding with a diameter of 128 μm and a numerical aperture (NA) of 0.45 serves as the gain fiber. A 793 nm diode laser (BWT) with a max output power of 6 W is used to pump the gain fiber through a $(2+1)\times 1$ pump combiner (ITF, Canada). A 10% port of a 10/90 fiber coupler centered at 2 μm is used to output the laser from the cavity. A polarization-independent optical isolator with an insertion loss of 0.76 dB at 2 μm (Advanced Photonics, USA) is adopted to ensure the unidirectional propagation. The well-prepared AFLF connected between two polarization controllers (PCs) is used to introduce both the NPE effect and filtering effect. An SWCNT sandwiched between two optical ferrules is used as a slow SA to achieve mode-locked self-starting [1]. The measured modulation depth, nonsaturable loss, and saturable peak intensity of the SWCNT SA are 21.2%, 59.6%, and 2.23 MW/cm^2, respectively. The hybrid mode-locked mechanism that incorporates both "slow" and "fast" SAs permits generating self-starting ultrashort pulses with narrower pulse duration [11,12]. The total fiber laser cavity is ~12.6 m, including 2.0 m of Tm-doped fiber and 10.6 m of SMF-28e pigtail fiber. The anomalous dispersion values of the Tm-doped fiber and the SMF-28e fiber at 1.9 μm are about −84 ps^2/km and −80 ps^2/km, respectively. The net dispersion in the cavity is thus estimated to be −1.176 ps^2, indicating that the laser is operating in an anomalous dispersion regime. Temporal and spectral profiles of the output pulses are, respectively, monitored by an InGaAs photodetector (EOT ET-5000F, USA) followed by a 500 MHz digital oscilloscope and an optical spectrum analyzer (Yokogawa AQ6375) with resolution of 0.05 nm. The pulse duration is measured by an interference autocorrelator (APE, Germany).

4. EXPERIMENT AND SIMULATION RESULTS

We investigate the AFLF-based mode-locked oscillator by adjusting the PC and pump power where the FSR of the AFLF is 20.8 nm. A stable self-starting single-soliton pulse is formed at the pump power of 1.38 W. A pulse break occurs as the pump power increases to 1.53 W. Since we focus on the filtering of the Kelly sidebands, the pulse spectrum evolution is observed in detail (Visualization 1). Initially, stable soliton pulses without Kelly sidebands are generated at the pump of 1.38 W. As the pump power ramps up, the spectral intensity and full width at half-maximum (FWHM) gradually increase, and Kelly sidebands emerge and increase around the center wavelength of 1966.4 nm. The Kelly sidebands reach their highest intensity at the critical condition of soliton splitting. Figure 3(a) shows the spectrum in this case (see spectrum_A). The measured FWHM and center wavelength are 3.8 nm and 1966.4 nm, respectively. The intensity difference between the peak of the first-order Kelly sideband at 1960.35/1972.9 nm and center peak of the soliton is up to 15 dB. Here the AFLF with an FSR of 20.8 nm is used to suppress the Kelly sidebands. Although the AFLF with a narrower FSR is more favorable for suppressing Kelly sidebands, the spectrum width of the soliton is reduced and thus leads to a change of pulse duration. By comparing AFLFs with different FSRs of 15.0 nm, 20.8 nm, and 25.0 nm, we find that, if the FSR of the AFLF is nearly five times as much as the pulse spectral FWHM without an AFLF, the main part of the Kelly sidebands will be suppressed without changing pulse duration. The blue curve in Fig. 3(a) shows the spectral response of the AFLF. The transmission difference at the center wavelength of 1966.4 nm and wavelength of the first-order Kelly sideband is 6.0 dB, indicating that the first-order Kelly sideband is indeed weakened by the AFLF. Further suppression of first-order Kelly sidebands is limited mainly by the low modulation depth of the AFLF, which is determined by the low polarization extinction ratio (PER) of the 45°-TFG in our case, since the splicing angle between the 45°-TFG and PMF cavity is set at the optimal 45°. Since the center wavelength of the phase mask for our 45°-TFG fabrication is at 1.9 μm instead of 2 μm, the 45°-TFG has a low PER of ~10 dB around 2 μm. If a new phase mask centered at 2 μm is used in the near future, a higher PER of >20 dB can be obtained. Thus, high modulation depth is expected for further suppressing both the first- and second-order Kelly sidebands.

To better verify the function of the AFLF on the suppression of Kelly sidebands, we replace the AFLF with a commercial polarizer centered at the 2 μm band, and their cavity lengths are the same. The polarizer has an insertion loss of 3.4 dB at 2 μm. In this case, the self-starting and splitting thresholds of the single-soliton pulses, respectively, increase to 1.40 W and 1.55 W due to the large insertion loss of 3.4 dB of the polarizer. Spectrum_B in Fig. 3(a) is the soliton spectrum at the pump power of 1.55 W, where the Kelly sidebands are far stronger than in the soliton spectrum with the AFLF. In particular, the strongest Kelly sideband at 1972 nm is suppressed over 20.3 dB when the AFLF is used. The ASE intensity of spectrum_A is also less than that of spectrum_B because a part of the ASE light is also filtered out by the AFLF. The measured average powers of pulses with/without the AFLF are 1.37/1.62 mW, respectively, which is caused mainly by the intensity difference of the Kelly sidebands and ASE light between spectra_A and spectra_B. Figure 3(b) shows the autocorrelation traces corresponding to spectra_A and spectra_B in Fig. 3(a). Their FWHMs are nearly equal to 1.84 ps, and the same pulse

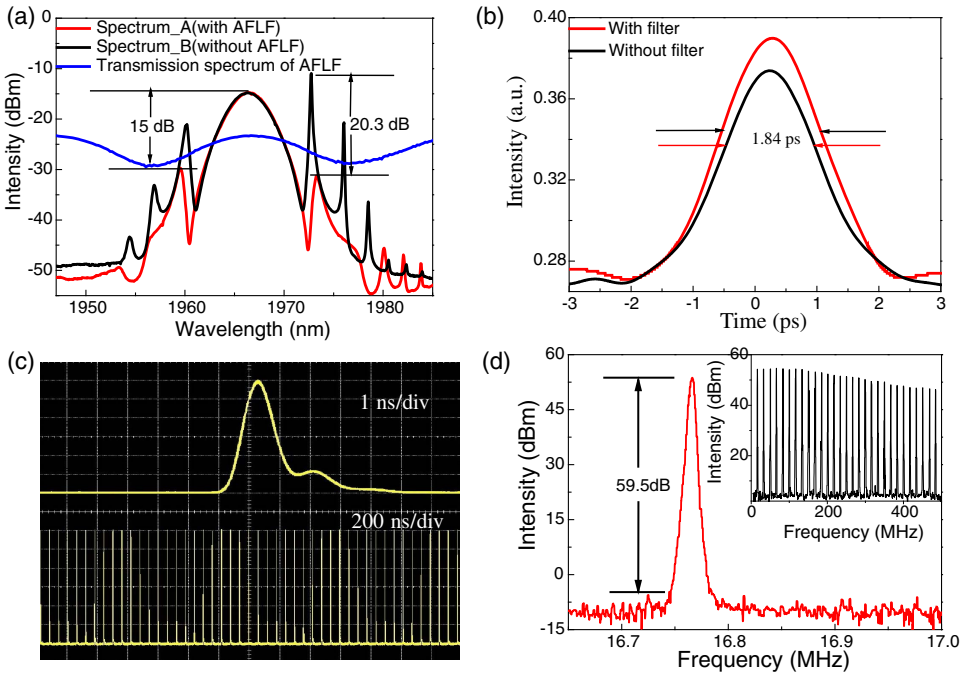

Fig. 3. Performances of mode-locked fiber lasers based on the AFLF with an FSR of 20.8 nm: (a) spectra from seed lasers with/without the AFLF, (b) autocorrelation traces corresponding to (a), (c) pulse waveform and sequence on oscilloscope, and (d) RF spectra with scanning range of 50 kHz and 500 MHz (inset).

duration of 1.18 ps is estimated with sech^2-pulse assumption. Consequently, their calculated time bandwidth products are all 0.339, indicating that they are chirp free. Figure 3(c) shows the oscilloscope trace of a single pulse and the pulse sequence of the AFLF-based fiber laser at the pump power of 1.52 W. The measured repetition rate of 14.12 MHz matches well with the cavity-length-dependent theoretical value. Figure 3(d) shows the corresponding radio frequency (RF) spectrum of the output pulses with a scanning range of 350 kHz and a resolution of 3 kHz. The high signal-to-noise ratio of ~59.5 dB and the absence of modulation in the 500 MHz broad RF spectrum [see inset of Fig. 3(d)] indicate the good stability and uniformity of the mode-locked oscillator.

We investigate the wavelength tunability of the AFLF by changing its temperature. Figure 4(a) shows the theoretically calculated transmission spectra of the AFLF according to Eq. (8) with 50 cm PMF. It is observed that the transmission spectrum within the range of 1930–1990 nm blue-shifts from 1969.9 nm to 1952.1 nm with increased temperature from 10°C to 60°C. Moreover, the wavelength shift of the transmission spectrum of the AFLF with respect to that at room temperature set as 24°C is also calculated versus the temperature and displayed in Fig. 4(b). Note that the PMF length under heating in this case is set as 7 cm to match our experimental value. It is seen that the wavelength shift linearly varies from 4.98 nm to −12.82 nm with increased temperature from 10°C to 60°C, giving a temperature tuning responsivity of −0.356 nm/°C. This provides a simple, cost-effective, and high-sensitivity method to realize laser wavelength tuning. Accordingly, a heating device is introduced into the mode-locked Tm-doped fiber laser cavity to control the temperature of the PMF and thus tune the laser wavelength. Since the spectrum response of the AFLF is independent of the polarization state of the laser, the soliton can be precisely tuned without adjusting the PCs. Figure 4(c) shows the spectra of the mode-locked pulses by changing the temperature from 7°C to 60°C. As expected, the blue-shifted spectrum shows that well-suppressed Kelly sidebands with increased temperature from 7°C to 60°C are achieved. The center wavelength decreases from 1971.62 nm to 1952.63 nm as shown in Fig. 4(d), giving a temperature tuning responsivity of −0.359 nm/°C, matching the theoretically calculated results, as shown in Figs. 4(a) and 4(b). Therefore, the maximum continuous wavelength tunable range of ~19 nm is obtained. Once the temperature is adjusted beyond the above range (i.e., 7°C–60°C), the spectrum of the mode-locked pulses will jump to the red tuning edge for the case above 60°C and blue tuning edge for the case below 7°C, respectively, corresponding to the adjacent filtering channels of the AFLF as a result of intra-cavity gain competition. In our experiment, wavelength tuning is almost synchronous when the temperature is changed at a rate of 0.3°C/s. Thus, the total tuning time is about 3 min, which will be finally limited by the rate of fiber heat conduction. Moreover, it is also found that the tuned wavelength always corresponds to a certain temperature, no matter how the temperature is changed, indicating good repeatability of the tuning method based on the AFLF. Further extension of the wavelength tuning range can result in a two- or multi-stage AFLF owing to its larger FSR. When the heating device is turned off, the obtained center wavelength of 1966.45 nm suggests the room temperature in our lab is 21.87°C according to the linear relationship in Fig. 4(d). This method can also be employed for accurate temperature measurement.

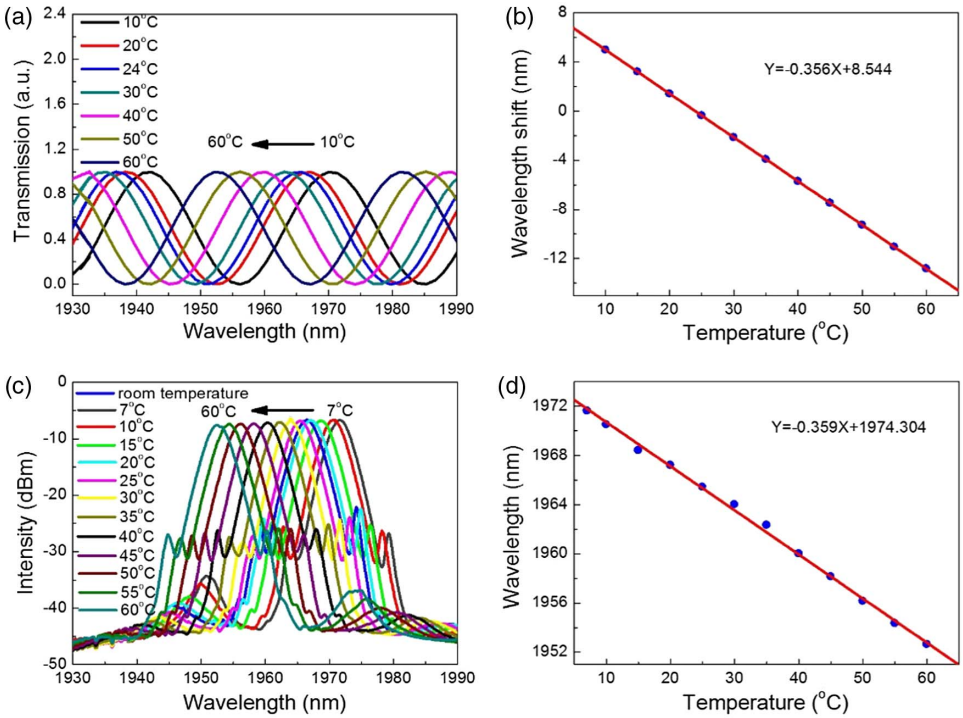

Fig. 4. (a) Theoretically calculated transmission spectra of the AFLF at different temperatures, (b) theoretically calculated wavelength shift of the AFLF as a function of temperature, (c) experimentally measured spectra at different temperatures, and (d) experimentally measured center wavelength as a function of temperature.

5. DISCUSSION

In our system, mode-locked pulses with well-suppressed Kelly sidebands are obtained using the AFLF with an optimized PMF length of 50 cm. The experimental results show that a longer PMF (i.e., a smaller bandwidth of the AFLF) leads to a narrower spectrum bandwidth and hence introduces additional chirp. In contrast, a shorter PMF (i.e., a larger bandwidth of the AFLF) exhibits a weak ability to suppress Kelly sidebands. Therefore, it is concluded that when the maximum transmission of the AFLF matches the center of the spectrum while its two adjacent minimum transmissions are located at the first-order Kelly sidebands, the best filtering performance is obtained. This rule can be used to design the AFLF according to a practical soliton spectrum. Moreover, the tunable range of ~19 nm for mode locking is achieved by varying temperature from 7°C to 60°C. Further broadening of the tunable range is limited mainly by the small FSR of our used AFLF, which makes the interference of adjacent filtering channels easier during wavelength tuning. Therefore, if the FSR of the AFLF can be increased while keeping its optimized bandwidth, a broader tunable range for mode locking is expected without impairing suppression of the Kelly sidebands. The multi-stage AFLF is an available approach to realize this goal. Since the bandwidth and FSR of the multi-stage AFLF are determined by the longest and shortest PMFs, respectively, a small bandwidth and a large FSR can be obtained simultaneously.

6. CONCLUSION

In this paper, we report the generation of a conventional soliton with precise wavelength tunability and suppressed Kelly sidebands in a Tm-doped mode-locked fiber laser by designing a 45°-TFG-based AFLF. The AFLF, first fabricated at the 2 μm band, shows advantages of controllable FSR, large filtering depth of ~9 dB, precise wavelength tunability, small insertion loss, and compact structure. Benefiting from the AFLF, the Kelly sidebands of the conventional soliton is dramatically weakened over 20 dB, and the laser wavelength can be precisely tuned from 1971.62 nm to 1952.63 nm. The AFLF also serves as a polarizer to induce the NPE effect, which combined with a slow SA (SWCNT) ensures the self-starting and stability of the soliton mode locking.

Funding. National Natural Science Foundation of China (NSFC) (614350003, 61722503, 61421002); Open Fund of Science and Technology on Solid-State Laser Laboratory; Fundamental Research Funds for the Central Universities (ZYGX2016J068); International Scientific Cooperation Project of Sichuan Province (2017HH0046); Joint Fund of Ministry of Education for Equipment Pre-research (6141A02033411).

REFERENCES

1. J. Bogusławski, G. Soboń, R. Zybała, K. Mars, A. Mikuła, K. M. Abramski, and J. Sotor, "Investigation on pulse shaping in fiber laser hybrid mode-locked by Sb_2Te_3 saturable absorber," Opt. Express **23**, 29014–29023 (2015).
2. Z. Sun, T. Hasan, F. Wang, A. G. Rozhin, I. H. White, and A. C. Ferrari, "Ultrafast stretched-pulse fiber laser mode-locked by carbon nanotubes," Nano Res. **3**, 404–411 (2010).
3. Z. Sun, D. Popa, T. Hasan, F. Torrisi, F. Wang, E. J. R. Kelleher, J. C. Travers, V. Nicolosi, and A. C. Ferrari, "A stable, wideband tunable,

near transform-limited, graphene-mode-locked, ultrafast laser," Nano Res. **3**, 653–660 (2010).
4. C. Zhao, Y. Zou, Y. Chen, Z. Wang, S. Lu, H. Zhang, S. Wen, and D. Tang, "Wavelength-tunable picosecond soliton fiber laser with topological insulator: Bi_2Se_3 as a mode locker," Opt. Express **20**, 27888–27895 (2012).
5. J. Sotor, G. Sobon, M. Kowalczyk, W. Macherzynski, P. Paletko, and K. M. Abramski, "Ultrafast thulium-doped fiber laser mode locked with black phosphorus," Opt. Lett. **40**, 3885–3888 (2015).
6. H. Haus, "Theory of mode locking with a slow saturable absorber," IEEE J. Quantum Electron. **11**, 736–746 (1975).
7. F. X. Kurtner, J. A. der Au, and U. Keller, "Mode-locking with slow and fast saturable absorbers-what's the difference?" IEEE J. Sel. Top. Quantum **4**, 159–168 (1998).
8. B. Farrow and P. V. Kamat, "CdSe quantum dot sensitized solar cells. Shuttling electrons through stacked carbon nanocups," J. Am. Chem. Soc. **131**, 11124–11131 (2009).
9. M. E. Fermann and I. Hartl, "Ultrafast fiber laser technology," IEEE J. Sel. Top. Quantum **15**, 191–206 (2009).
10. L. E. Nelson, D. J. Jones, K. Tamura, H. A. Haus, and E. P. Ippen, "Ultrashort-pulse fiber ring lasers," Appl. Phys. B **65**, 277–294 (1997).
11. M. Guina, N. Xiang, A. Vainionpää, O. G. Okhotnikov, T. Sajavaara, and J. Keinonen, "Self-starting stretched-pulse fiber laser mode locked and stabilized with slow and fast semiconductor saturable absorbers," Opt. Lett. **26**, 1809–1811 (2001).
12. S. Kim, Y. Kim, J. Park, S. Han, S. Park, Y. J. Kim, and S. W. Kim, "Hybrid mode-locked Er-doped fiber femtosecond oscillator with 156 mW output power," Opt. Express **20**, 15054–15060 (2012).
13. Q. Wang, J. Geng, T. Luo, and S. Jiang, "2 μm mode-locked fiber laser," Proc. SPIE **8237**, 82371N (2012).
14. S. Kelly, "Characteristic sideband instability of periodically amplified average soliton," Electron. Lett. **28**, 806–807 (1992).
15. J. Li, Z. Yan, Z. Sun, H. Luo, Y. He, Z. Li, Y. Liu, and L. Zhang, "Thulium-doped all-fiber mode-locked laser based on NPR and 45°-tilted fiber grating," Opt. Express **22**, 31020–31028 (2014).
16. R. Weill, A. Bekker, V. Smulakovsky, B. Fischer, and O. Gat, "Spectral sidebands and multipulse formation in passively mode-locked lasers," Phys. Rev. A **83**, 043831 (2011).
17. M. L. Dennis and I. N. Duling, "Experimental study of sideband generation in femtosecond fiber lasers," IEEE J. Quantum Electron. **30**, 1469–1477 (1994).
18. C. W. Rudy, K. E. Urbanek, M. J. F. Digonnet, and R. L. Byer, "Amplified 2-μm thulium-doped all-fiber mode-locked figure-eight laser," J. Lightwave Technol. **31**, 1809–1812 (2013).
19. M. E. Fermann, M. J. Andrejco, M. L. Stock, Y. Silberberg, and A. M. Weiner, "Passive mode locking in erbium fiber lasers with negative group delay," Appl. Phys. Lett. **62**, 910–912 (1993).
20. M. Nakazawa, E. Yoshida, T. Sugawa, and Y. Kimura, "Continuum suppressed, uniformly repetitive 136 fs pulse generation from an erbium-doped fibre laser with nonlinear polarisation rotation," Electron. Lett. **29**, 1327–1329 (1993).
21. M. J. Guy, D. U. Noske, and J. R. Taylor, "Generation of femtosecond soliton pulses by passive mode locking of an ytterbium-erbium figure-of-eight fiber laser," Opt. Lett. **18**, 1447–1449 (1993).
22. D. U. Noske and J. R. Taylor, "Spectral and temporal stabilisation of a diode-pumped ytterbium-erbium fibre soliton laser," Electron. Lett. **29**, 2200–2202 (1993).
23. K. Tamura, C. R. Doerr, H. A. Haus, and E. P. Ippen, "Soliton fiber ring laser stabilization and tuning with a broad intracavity filter," IEEE Photon. Technol. Lett. **6**, 697–699 (1994).
24. L. Yun, X. Liu, and D. Mao, "Observation of dual-wavelength dissipative solitons in a figure-eight erbium-doped fiber laser," Opt. Express **20**, 20992–20997 (2012).
25. S. Huang, Y. Wang, P. Yan, J. Zhao, H. Li, and R. Lin, "Tunable and switchable multi-wavelength dissipative soliton generation in a graphene oxide mode-locked Yb-doped fiber laser," Opt. Express **22**, 11417–11426 (2014).
26. K. Kieu and M. Mansuripur, "Tuning of fiber lasers by use of a single-mode biconic fiber taper," Opt. Lett. **31**, 2435–2437 (2006).
27. Y. Wang, J. Li, B. Zhai, Y. Hu, K. Mo, R. Lu, and Y. Liu, "Tunable and switchable dual-wavelength mode-locked Tm^{3+}-doped fiber laser based on a fiber taper," Opt. Express **24**, 15299–15306 (2016).
28. X. Liu, D. Han, Z. Sun, C. Zeng, H. Lu, D. Mao, Y. Cui, and F. Wang, "Versatile multi-wavelength ultrafast fiber laser mode-locked by carbon nanotubes," Sci. Rep. **3**, 2718 (2013).
29. Z. Yan, C. Mou, H. Wang, K. Zhou, Y. Wang, W. Zhao, and L. Zhang, "All-fiber polarization interference filters based on 45°-tilted fiber gratings," Opt. Lett. **37**, 353–355 (2012).
30. Z. Yan, H. Wang, K. Zhou, Y. Wang, W. Zhao, and L. Zhang, "Broadband tunable all-fiber polarization interference filter based on 45° tilted fiber gratings," J. Lightwave Technol. **31**, 94–98 (2013).
31. Z. Yan, H. Wang, K. Zhou, Y. Wang, C. Li, W. Zhao, and L. Zhang, "Soliton mode locking fiber laser with an all-fiber polarization interference filter," Opt. Lett. **37**, 4522–4524 (2012).
32. K. Özgören and F. Ö. Ilday, "All-fiber all-normal dispersion laser with a fiber-based Lyot filter," Opt. Lett. **35**, 1296–1298 (2010).